Final Report

Final Report for Austrian Marshall Plan Scholarship

Title of Research Project

"Experimental and Numerical Simulation of Burst Experiment for Determining Fracture Toughness under Confining Pressure"

Research Scholar full name: Onur Inal

Supervisor at home university: Assoc. Prof. Marlène Villeneuve, PhD, FHEA

Co-supervisor at home university: Univ.-Prof. PhD Keita Yoshioka

Co-supervisor at host university: Assoc. Prof. Andrew Bunger

25.03.2024

ABSTRACT

The burst experiment is a common method that is mostly used in the petroleum industry to estimate the fracture toughness (K_{IC}) of rocks under confinement in the laboratory. Unlike other methods, it tests rock samples subjected to confining stress, which represents the actual subsurface condition of a stressed wellbore with bi-wing fractures, and therefore it is considered advantageous to other methods. Fracture propagation in this burst experiment is only indicated by a sudden burst of the jacketed sample, where the burst pressure is measured. The fracture toughness of the sample can then be calculated after taking this recorded pressure as the critical pressure required to propagate the axially pre-notched wing fractures. However, the fracture growth may exist before the sample bursts, which might be a possible weakness of this technique. The cause is the existence of stable crack growth before the unstable "burst". Due to the challenges in the detection of this stable crack growth, there is significant uncertainty in the crack length used in the analysis of the results.

The purpose of this thesis is to estimate fracture toughness accurately by comparing the stable and unstable behavior types from numerical modeling predictions with the results of a series of modified burst experiments using acoustic emission (AE) detection for certain configurations. The results indicate that stable growth will occur before sample rupture for certain sample geometry and loading combinations. The difference between stable and unstable growth cases is detected from acoustic emission monitoring records. Moreover, modifications are proposed for more accurate fracture toughness calculations after investigating the behavior of the estimated fracture toughness results. More consistent estimations of fracture toughness are obtained from experiments with unstable configurations. The results of experiments with unstable behavior indicate a positive correlation between confining pressure and fracture toughness estimations, which complies with many observations reported in the literature. Lastly, fixed confinement experiments are performed for a legitimate calculation of K_{IC} with a range of geometry and loading conditions based on the global stability criterion. The effect of fixed confining pressure on the fracture toughness estimations has been shown, offering guidance for improved design of this frequently used test method.

TABLE OF CONTENTS

LIST OF TABLES

LIST OF FIGURES

1 INTRODUCTION

Rock fracturing has always been one of the most important topics in rock mechanics, and fracture networks play a key role, particularly in geothermal energy production, storing carbon dioxide (CO_2), and nuclear waste disposal in underground structures. Fracture toughness, as a material property, is a crucial factor in the evaluation of the fracturing of brittle rock. The toughness of a rock is a measure of its ability to withstand fracturing. In other words, a rock with high toughness requires a substantial amount of energy to experience failure; a considerable amount of energy is absorbed by a rock with high toughness when it fractures. One of the most often used methods for determining the fracture toughness of rocks under confinement pressure is the burst experiment in the laboratory (Abou-Sayed, 1978). To perform this test, a hollowed-out cylindrical sample with two wing cracks is subjected to radial confinement on the boundary while a simultaneous interior pressure is applied. The inner and outer pressures (P_i and P_o) are increased proportionally until the sample bursts.

The burst experiment is carried out on a thick-walled cylindrical sample with axial bi-wing notches to simulate fracture initiation, and then the fracture toughness estimation procedures are followed. Bowie & Freese (1972) determined the stress intensity factor numerically at the crack tip using "modified mapping-collacation" technique. In their study, researchers benefit from the assumption of orienting the x and y axes in such a way that they coincide with the principle planes of elastic symmetry of the orthotropic plate, which enables them to simplify the constitutive equations. Under this assumption, an Airy stress function for plane symmetric loading defines the stress intensity factor. In the following years, Clifton et al. (1976) performed a series of experiments on various rock samples (sandstone, siltstone, and shale) to estimate fracture toughness, applying closed-form approximations of the stress intensity factor for simple geometries and load cases in addition to numerical simulations. These studies form the basis, respectively, for subsequent stress intensity factor and fracture toughness estimations in Abou-Sayed (1978).

Over the years, it has been found that the fracture toughness of rocks under confining pressure can be significantly increased compared to the laboratory results of unconfined testing.

Yoshioka et al. (2023) and Zhang (2019) have also carried out a series of burst experiments using different configurations to better understand crack propagation and fracture toughness estimation. Figure 1.1 illustrates a combination of published results that demonstrate a positive correlation between confining stress and fracture toughness.

However, Yoshioka et al. (2023)have numerically and experimentally demonstrated that the burst experiment may be essentially dependent on the confining stress in a way that is not taken into account in the analysis of the experimental data. They have shown that the modified test configuration in an unstable manner allows researchers to detect the onset of crack propagation earlier than the original test setup, which was deliberately designed to obtain stable crack growth. Hence, it was demonstrated that more accurate fracture toughness estimation is possible with proposed modifications, whereas the fracture toughness may be systematically overestimated in the original burst experiment configuration. This approach requires further investigation through additional experiments (with stable and unstable designs) to assess the feasibility and accuracy of the burst experiment. In other words, the stability and reliability of the burst experiment should be investigated in a more comprehensive manner. This thesis aims to improve both the feasibility and accuracy of the burst experiment test using numerical and experimental techniques to perform additional experiments with various configurations. Thus, a more accurate estimation of the fracture toughness is achieved.
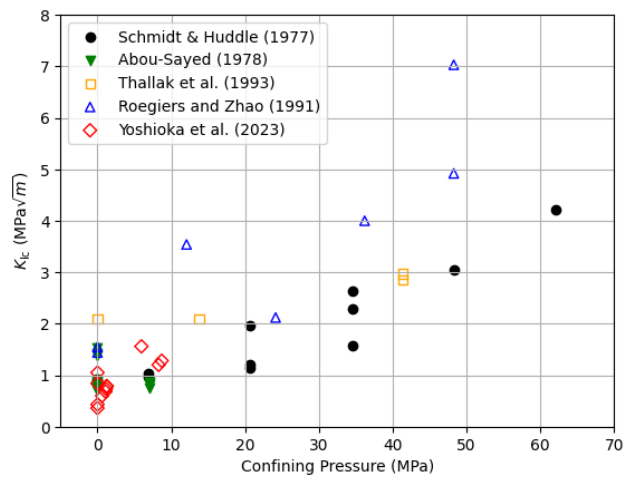
Figure 1.1: Fracture toughness vs confining pressure of Indiana Limestone (after Yoshioka et al., 2023)

1.1 Motivation

Rock fracture toughness has been measured using different experimental techniques, including the single-edge-notch test, the three-point-bending test, the confined cylindrical cell, the chevron-notched disk specimen (CDISK), and the beam test. These tests show a positive correlation between confining stress and fracture toughness. The burst experiment is the most popular laboratory test commonly applied in the oil and gas industry to estimate fracture toughness under confining pressure (Abou-Sayed, 1978). However, the recent studies of Yoshioka et al. (2023) and Zhang (2019) have analyzed the accuracy of this well-known test method and demonstrated some potential inaccuracies in the fracture toughness estimation. Yoshioka et al. (2023) have modified the current burst experiment configuration to have more accurate fracture toughness measurements. They have used the $G - \theta$ method to calculate the stress intensity factor numerically and set the experimental geometry and stress conditions such that the fractures occur in an "unstable" manner. During the laboratory tests, the acoustic emission monitoring method is implemented to demonstrate that stable crack propagation normally occurs well before the final failure. This situation leads to an overestimation of fracture toughness when it is calculated using the peak pressure result according to the original test procedure. All these questions and recent developments related to the accuracy of burst experiments necessitate the need to obtain more experimental data. In other words, the accuracy and reliability of the burst experiment should be investigated in a more comprehensive manner. In this sense, this thesis presents results from numerical and experimental simulations of the burst experiment. The numerical analysis method is used to calculate the stress intensity factor, applying different loading and geometrical configurations as an initial step to fracture toughness estimation. Eventually, a series of burst experiments are performed in the laboratory with different configurations, similar to recent studies, to assess the feasibility and accuracy of the facture toughness estimations on limestone samples under confining pressure. In some cases, acoustic emission monitoring is used to better understand crack growth mechanisms and to improve the accuracy of fracture toughness estimation with burst experiments.

1.2 Objectives

In recent years, the stability and reliability of this burst experiment testing method have been a matter of discussion in the rock mechanics community.

The primary objective is to analyze the reliability of burst experiments by implementing stable and unstable test configurations with specific combinations of sample geometry and loading conditions for the estimation of more accurate fracture toughness under confining pressure.

The second objective is to produce more reliable fracture toughness estimation results to compare both stable and unstable configuration results with the recent studies.

The third objective is to observe experimental behavior in both stable and unstable configurations. Some of the experiments are planned with acoustic emission monitoring to detect the actual onset of crack propagation.

The fourth objective is to investigate the effect of confining pressure on fracture toughness estimation in both fixed confinement and burst experiments.

2 THEORETICAL BACKGROUND

Think of a cylinder rock sample placed in the center of a burst cell. There are diametrically opposed initial notches along the central borehole. The confining pressure, P_o, is applied to the outside surface of the borehole, while the inner pressure, P_i, is applied inside the borehole.

At the beginning of the burst experiment, the pressure is increased simultaneously and proportionally, with p^* remaining constant, until a pressure drop is observed and the sample bursts. The pressure data is recorded, and the peak pressure is chosen to estimate the fracture toughness. A 2D sketch of the burst experiment sample geometry and applied pressures is shown from the top view in Figure 2.1.
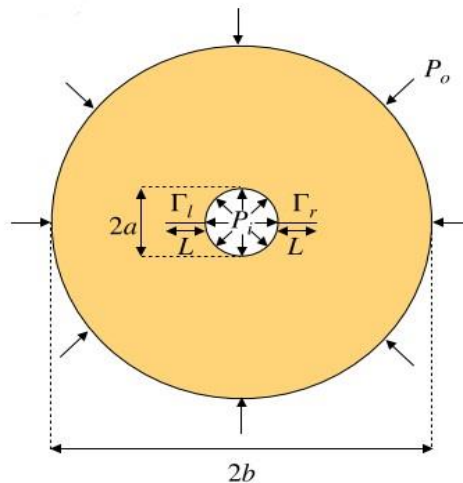
Figure 2.1: 2D sketch of the burst experiment sample and applied pressures

2.1 Fracture Toughness Estimation

Fracture toughness (K_{IC}) is a critical material property for fracture mechanics that indicates the amount of stress needed to propagate a preexisting flaw. Griffith (1921) conducted a sequence of experiments, analyzed stress, and integrated previous research in his exceptional paper to establish the fundamental concept that forms the basis of the contemporary theory of linear elastic fracture mechanics (LEFM). Griffith's energy relationship is founded upon the principles of linear elasticity theory, which predicts that stress at the tip of a sharp flaw in a linear elastic material is infinite. A few years later, he stated that a crack will propagate when the potential

energy release rate (strain energy release rate) that occurs due to the crack growth is equal to or greater than the increase in surface energy due to the creation of new free surfaces (Figure 2.2) (Griffith, 1924). Although this theory is applicable to brittle materials such as glass fibers, the predicted surface energy is usually remarkably high, especially for ductile materials such as steel. It depends on a critical energy release rate, G_c, which is geometry-independent and thus a material property. When the application of load results solely in the initiation of the fracture without any shearing or tearing occurring, and when material damage is localized to a very small region near the crack tip, the energy criterion is almost equivalent to $K_I = K_{IC}$. In other words, fracture occurs when $K_I \geq K_{IC}$ (Irwin, 1957), where K_I is computed as the stress intensity factor and K_{IC} is the material fracture toughness. The critical energy release rate, G_c, can also be related to rock fracture toughness, K_{IC}, via Equation (2.1),

$$G_c = \frac{K_{IC}^2}{E'} \tag{2.1}$$

where E' = E for plane stress and E' = E/(1-v^2) for plane strain, where E is the Young's modulus and v is the Poisson's ratio.
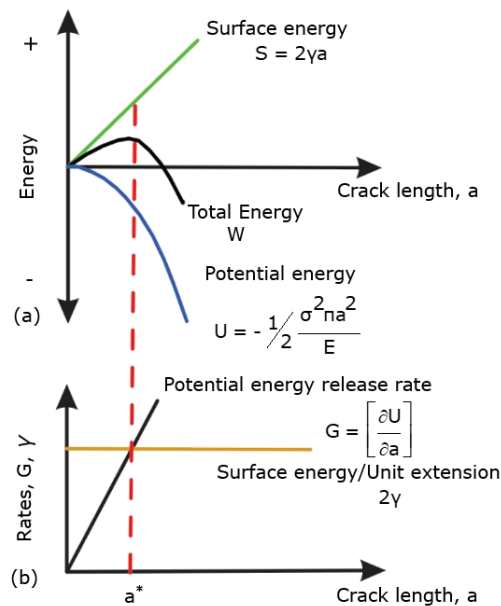
Figure 2.2: Diagram for the Griffith theory a) Variation of energy with crack length b) Variation of energy rates with crack length (a* is the critical Griffith crack length)

The stress intensity factor for an assumed straight crack of length 2a perpendicular to the loading direction in an infinite plane with a uniform stress field σ is given in Equation (2.2) (Figure 2.2).

$$K_I = \sigma\sqrt{\pi a} \qquad (2.2)$$
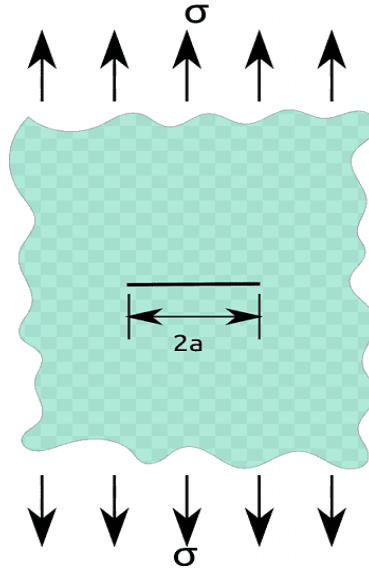
Figure 2.3: Crack in an infinite plate under mode I loading (URL-1)

When we focus on the development of K_I in relation to the length of fracture, $K_I(a,b,l_0,P_o,P_i)$ will be the stress intensity factor linked to a sample with an inner radius of a, an outer radius of b, an initial fracture length of l_0, and inner and outer pressures, respectively, P_i and P_o. Through the utilization of the stress field linearity in response to applied loads, and a simple alteration of scale, we can mathematically express the stress intensity factor, K_I, in relation to a non-dimensional stress intensity factor K_I (w, ℓ, p*),

$$= P_{ic}\sqrt{a\pi}\,K_I(w,\ell,p^*) \qquad (2.3)$$

where w, ℓ, p* are three non-dimensional parameters (Yoshioka et al., 2023)

$$w = \frac{b}{a} \quad p^* = \frac{P_o}{P_i} \quad \ell = \frac{l_0}{b-a} \qquad (2.4)$$

The ratio of the outer pressure to the inner pressure is $p*$, and the ratio of the outer radius to the inner radius is w. Normalized crack length is ℓ, where l_0 is the initial length of the notch.

Then, the critical stress intensity factor at which the crack propagates is defined as fracture toughness, denoted K_{IC}. Upon determining the burst pressure related to crack growth through experimentation, the fracture toughness K_{IC} for each experiment can be estimated by utilizing the equation introduced by Abou-Sayed (1978), that is

$$K_{IC} = P_{ic} \sqrt{a\pi} K_I \tag{2.5}$$

2.2 Fracture Propagation and Global Stability Criterion

The main emphasis of this section lies in analyzing the stability of fracture propagation within the burst experiment. The burst experiment was designed to estimate the resistance to fracturing K_{IC} (also known as fracture toughness) of rock samples having two notches of length l_0. This estimation is conducted under varying confining pressures, as it is a crucial parameter in determining the breakdown pressure during the mini-frac simulation. Different regimes of crack growth, namely stable and unstable, have been determined under the framework of linear elastic fracture mechanics. The calculation of these regimes depends on factors such as the confining pressure and geometry. When it comes to unstable crack propagation, the phase-field models for hydraulic fracturing do not provide relevant information (Tanné, 2017). Instead, we employ a stress intensity factor (SIF) analysis along the fracture path to ascertain the stability regimes of crack growth. In more recent studies, researchers have examined stable and unstable crack growth regimes, associating inner pressure, P_{ic}, with stress intensity factor analysis (Yoshioka et al., 2023; Huang et al., 2022).

> The challenge in interpretation arises from the potential inaccuracy of assuming that the burst pressure, P_{ic}, provides the necessary loading for the initial extension of a crack with a length of l_0. In reality, if there is stable crack growth prior to the sudden change in pressure leading to an eventual unstable "burst", the actual length of the crack at the time of the burst occurrence will be greater than what is predicted by the analysis. This will result in overestimating the fracture toughness and, hence, overstating the dependence of fracture

toughness on confinement. At this stage, three potential variations of K_I and the corresponding P_{ic} exist, which can be utilized to determine the stability of crack growth in the burst experiment (Huang et al., 2022).

(a) The K_I is experiencing a steady decrease with ℓ increasing, while the P_{ic} is an increasing function of the fracture length, ℓ (Figure 2.4a). This case leads to "stable" crack growth in the burst experiment.

(b) The K_I shows a fluctuation at the beginning and then increases with ℓ *increasing, while the P_{ic} also shows a fluctuation initially and then decreases with ℓ increasing* (see Figure 2.4b). The crack growth will exist either stably or unstably, depending on the normalized crack length ℓ.

(c) The K_I is increasing monotonically with ℓ increasing, while the P_{ic} is decreasing with ℓ increasing monotonically (Figure 2.4c). In this case, unstable crack growth is observed, so the sample will burst instantaneously due to the dynamic propagation.
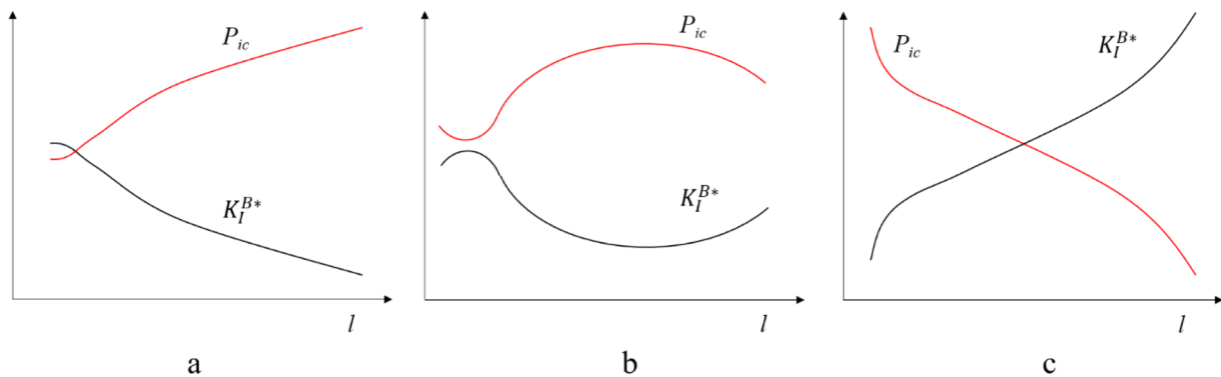
Figure 2.4: Evaluation of crack growth stability regimes (Huang et al., 2022)

2.3 SIF Calculation

The stress intensity factor (K_I) is defined as the stress state at a crack tip in fracture mechanics. The calculation of SIF is a significant step to show the influence of the test configuration, loads, and crack length upon the stresses near the end of the crack in brittle tensile fracture mechanics (Irwin, 1957). The simulation of burst SIF is a crucial step in the estimation of fracture toughness. Throughout this procedure, SIF is computed numerically using the $G - \theta$

method. In comparison to the J-integral technique, the G - θ method offers an alternative approach to determining the energy release rate in elastic, viscoplastic, or dynamic fractures. This method utilizes a surface integral, allowing for the determination of the energy release rate with a reasonable computational effort (Dubois et al., 1999).

When we consider the evolution of the non-dimensional stress intensity factor K_I (w, ℓ, p^*) with the crack length ℓ for the parameter analysis (w, p^*) in order to investigate the stability of crack propagation regimes, the burst problem denoted (B) is decomposed into the elementary problems applying Linear Elastic Fracture Mechanics (LEFM). Abou-Sayed (1978) has proposed an approach to decompose it into two problems following Figure 2.5: a situation where pressure is applied only to the inner cylinder, known as the jacketed problem (J), and the unjacketed problem (U) where the fluid exerts pressure on all internal sides. In this case, SIF is calculated as follows,

$$K_I(w, \ell, p^*) = K_I^J(w, \ell) - p^* K_I^U(w, \ell) \tag{2.6}$$

where $K_I^U(w, \ell) \geq 0$ for a positive P_o applied in the interior of the geometry.
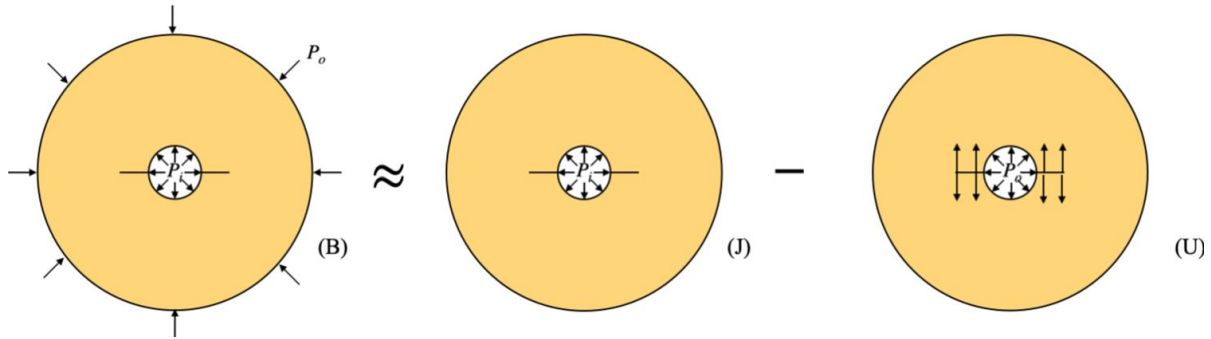
Figure 2.5: Superposition of the burst problem approximated in Abou-Sayed (1978)

However, in this study, the burst problem is decomposed into two problems following Tanné (2017): the superposition of jacketed test (J) and a constrained test (C), as illustrated in Figure 2.6 for a unit internal pressure. Similar to Abou-Sayed (1978), the pressure is applied only in the inner cylinder for the jacketed problem (J), whereas a constrained problem has only a confining

pressure applied on the outer cylinder named (C). Hence, the SIF for (B) can then be superposed as

$$K_I(w, \ell, p*) = K_I^J(w, \ell) + p * K_I^C(w, \ell) \qquad (2.7)$$

where $K_I^C(w, \ell)$ is positive for negative applied external pressure P_0.
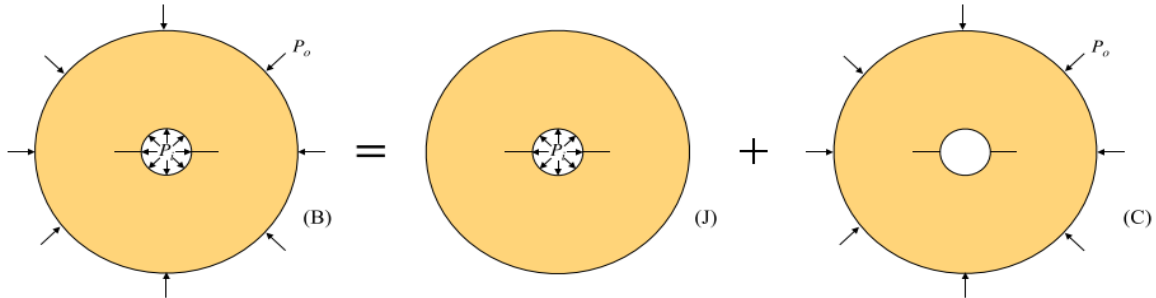
Figure 2.6: Decomposition of burst problem (B) into jacketed (J) and constrained (C) problems according to Tanné (2017)

Tanné (2017) decomposition does not consider pore pressure (P_p) within the sample, as a drain is employed to release the internal pressure within the rock.

In Figure 2.5, the results of $K_I^{J^*}$ and $K_I^{U^*}$ computation applying the G − θ method are closely aligned with the values reported by Clifton et al. (1976), indicating a strong agreement between the two sets of data. The G − θ approach is a calculation of the second derivatives of the potential energy concerning the crack length, achieved by implementing a virtual perturbation of the domain (vector θ) in the direction of crack propagation (Destuynder et al., 1981; Suo & Combescure, 1992). Then, the SIF is calculated using the Irwin formula (Equation(2.1)) based on the computed G.

Figure 2.7: Comparison of computed SIF evolution for the jacketed and unjacketed problems vs. normalized crack length ℓ. Colored lines numerical SIF computation results based on $G - \theta$ method (Yoshioka et al., 2023)

2.3.1 Numerical Simulation

Numerical simulation of the burst experiment enables researchers to compute SIF using the $G - \theta$ method, which is b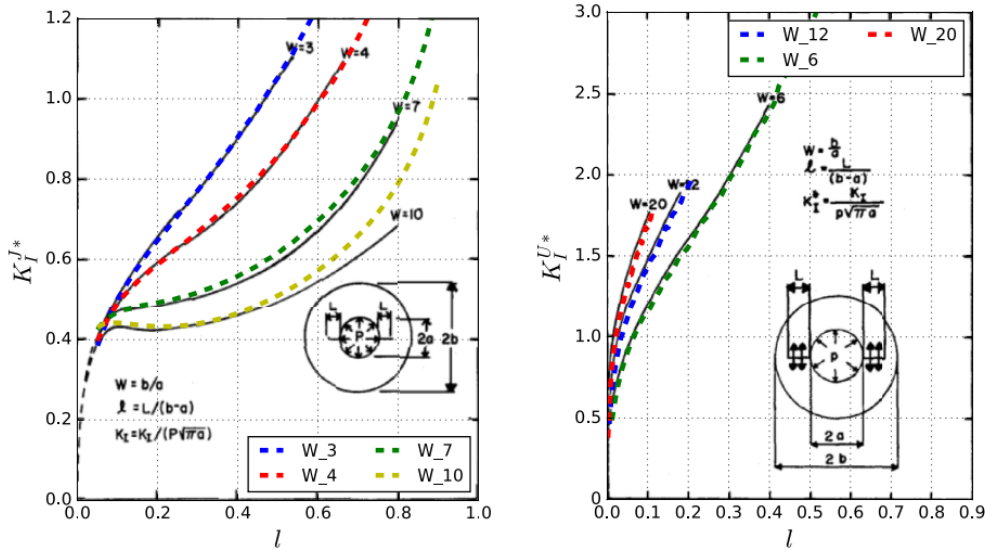eneficial compared to alternative methods. For this reason, a quarter model of the burst experiment has been simulated using OpenGeoSys (OGS), which is an open-source project for the development of numerical applications for the simulation of coupled thermo-hydro-mechanical-chemical (THMC) processes in porous and fractured media (URL-2).

The material behavior, model geometry, notch length, number of notches, loading and boundary conditions, and meshing have crucial roles in the quality of simulation results. The simulation strategy focuses on generating a tensile deformation at the crack tip for various configurations to calculate reliable SIF. Figure 2.8 shows the schematic structure of the model, which is described in detail below. The geometry and meshing of the model are generated via Gmsh, which is an open-source 3D finite element mesh generator with a built-in CAD engine and post-processor (URL-3). A quarter-burst experiment model is simulated using the symmetric modeling technique. This quarter model is simulated for seven different outer and inner diameter ratios (w3, w4, w6, w7, w10, w12, and w20). Following this, fifty different notch

lengths are simulated for each simulation on the horizontal axis. Eventually, G and SIF values are computed for these different notch lengths, respectively, and their trends are presented graphically by comparing them with normalized notch length in Section 2.4. Fine meshing is used along the notch length on the horizontal axis to obtain more reliable results.
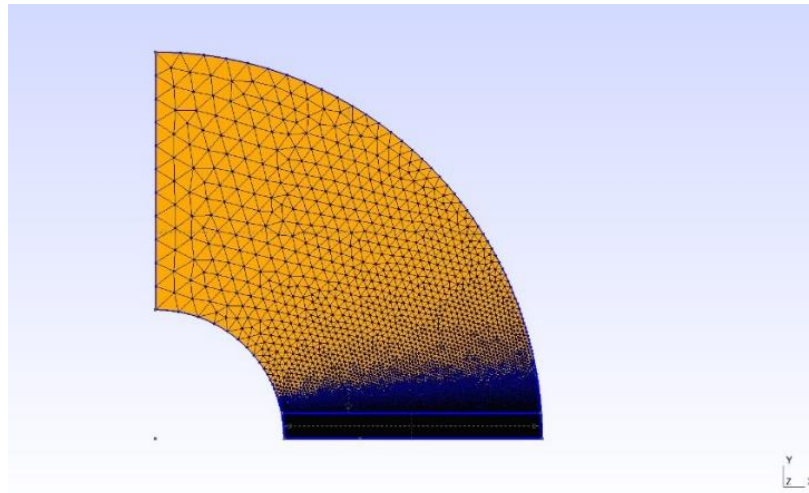

Figure 2.8: Principal sketch of the quarter model geometry and meshing in Gmsh

An attempt is made to compute jacketed (J) and constrained (C) approaches to the decomposed burst problem according to Tanné (2017) to obtain SIF results (explained in detail in Section 2.3). The models are simulated based on linear elastic material behavior and run using OGS. Then, the results are displayed and analyzed in ParaView, which is also an open-source platform to visualize and analyze modeling results. To simulate jacketed and constrained problems, inner and outer pressures are applied to the model, respectively. Restraint boundary conditions are applied on the horizontal axis immediately after the notch and on the vertical axis. No boundary restriction is applied to the outer surface in jacketed cases where internal pressure is applied, while the inner surface boundary was not restrained in the constrained problem where external pressure was applied. Figure 2.9 illustrates these applications together with a boundary condition on a model having displacement in X and Y directions in ParaView.
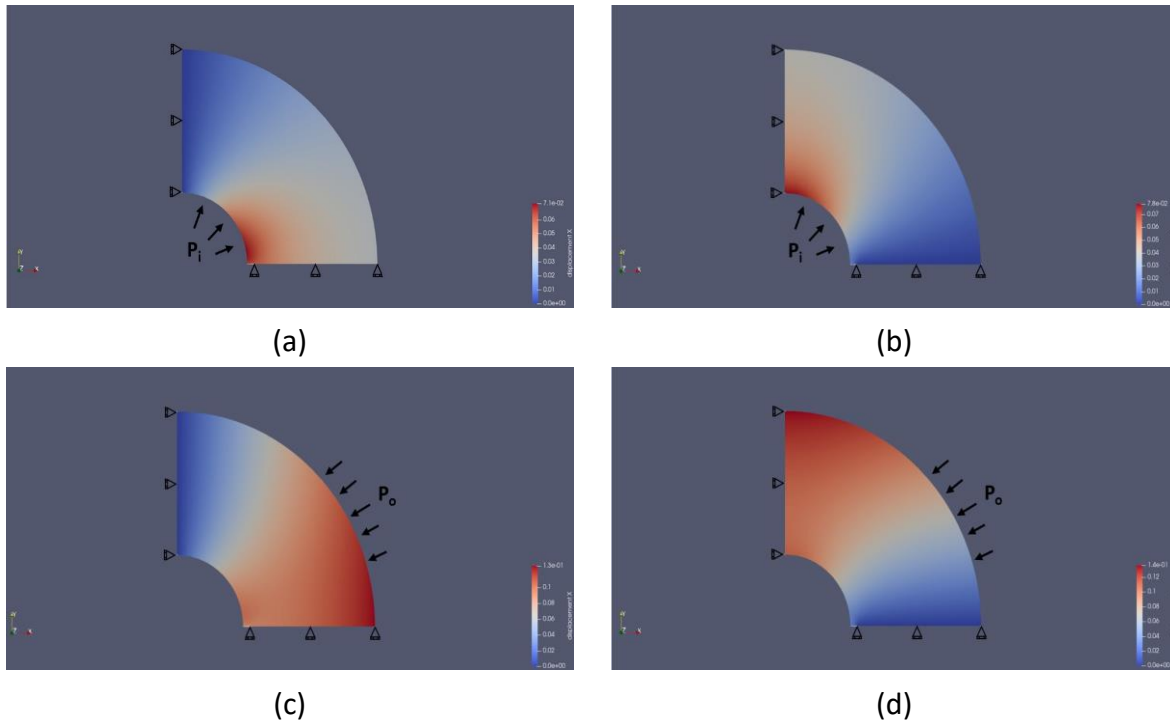
Figure 2.9: Boundary and loading conditions for jacketed and constrained problems, (a) Jacketed case displaced in X direction (b) Jacketed case displaced in Y direction (c) Constrained case displaced in X direction (d) Constrained case displaced in Y direction

2.3.2 SIF Results

The SIFs of both jacketed (J) and constrained (C) problems have been calculated numerically using the G − θ method as mentioned in Section 2.3. The results from the superposition of these two SIFs are shown in Figure 2.10-11 for $w = 3$ and $w = 12$ geometries. Furthermore, SIFs are computed and shown in Figure 2.12-13 for fixed confinement experiments, also having $w = 3$ and $w = 12$. In these simulation results, the four types of relationships between normalized SIF and non-dimensional notch length are shown. When K_I shows an upward trend with increasing normalized fracture length ℓ, unstable crack growth is expected in these cases based on the global stability criterion stated in Section 2.2. K_I increases generally in direct proportion to the initial notch length. If K_I shows a downward trend as opposed to the first case with increasing normalized fracture length ℓ, it is possible to expect pre-existing stable crack growth according to our hypothesis.

14

In order to calculate the fracture toughness with SIF simulation, the dimensionless initial notch length l_0 is fixed to 7.62 mm, which corresponds to ℓ = 0.11 for w =12 and ℓ = 0.15 for w =3. Therefore, the normalized value of K_I for each test can be estimated according to the simulation results as shown in Figure 2.10-13, corresponding to the values of p^* and w. K_{IC} can be estimated for each case based on these values and Equation (2.5), when the critical inner pressure is known at the point of rupture after each burst experiment in the following sections.
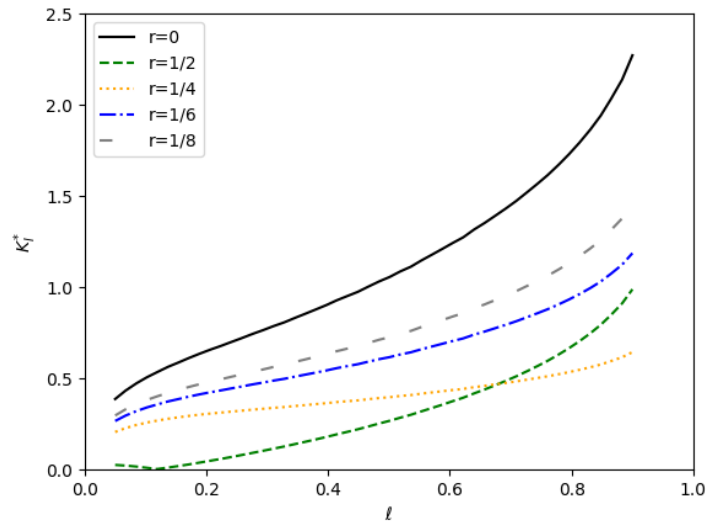

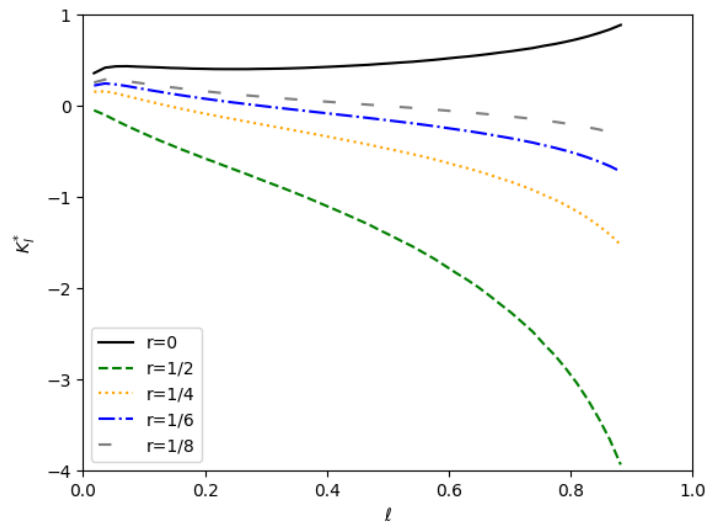Figure 2.10: Simulation results of K_I for w=3

Figure 2.11: Simulation results of K_I for w=12

15
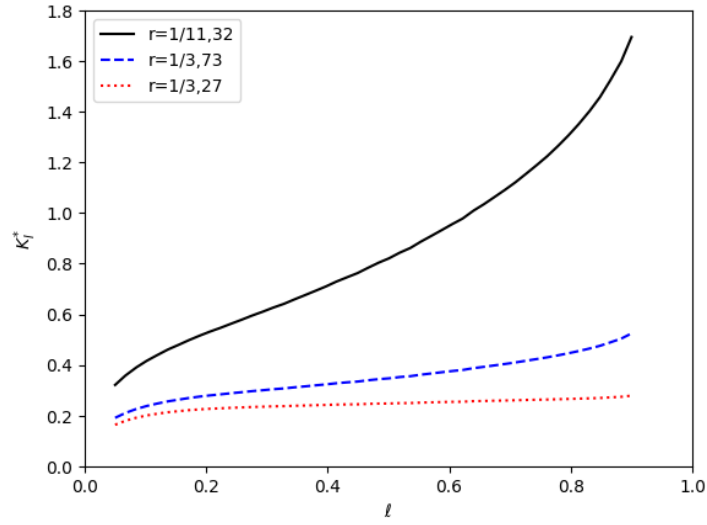
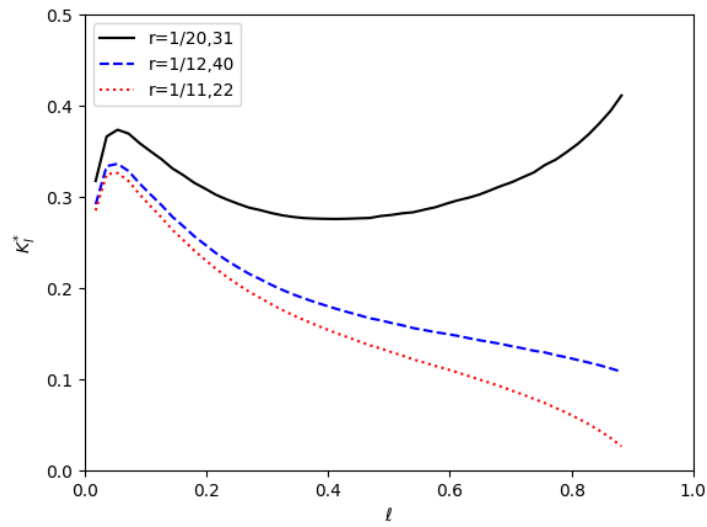Figure 2.12: Simulation results of K$_l$ for fixed confinement tests with w=3

Figure 2.13: Simulation results of KI for fixed confinement tests with w=12

3 EXPERIMENTAL SETUP

3.1 Apparatus and Design Configurations

The main component of the burst experiment is a burst cell, which is a conventional triaxial system. The setup for the burst experiment can be seen in Figure 3.1. The initial step in conducting a test involves placing the cylindrical rock sample at the center of a burst cell, which is surrounded by an oil-filled chamber to apply the confining pressure. There is an outer membrane that acts as a barrier and effectively prevents the infiltration of oil into the chamber. The sample is positioned at the vertical midpoint of the chamber using a pair of aluminum spacers (Figure 3.2a). A tygon tube, as shown in Figure 3.2(b), is inserted into the central hole of the sample, and sealed by two rubber plugs from top and bottom. The steel rod inside the tygon tube serves to keep the two rubber plugs in position, allowing them to expand by means of compression and thus improving the seal. This system allows for the application of internal pressure while simultaneously preventing the infiltration of fluid into the specimen. The internal pressure is applied by water, unlike the confinement pressure. The steel plate covers are secured in place using bolts at both the top and bottom to maintain the structural integrity of the system. Two ISCO syringe pumps are operated simultaneously to raise the inner pressure and the confining pressure proportionally until a pressure drop is observed.
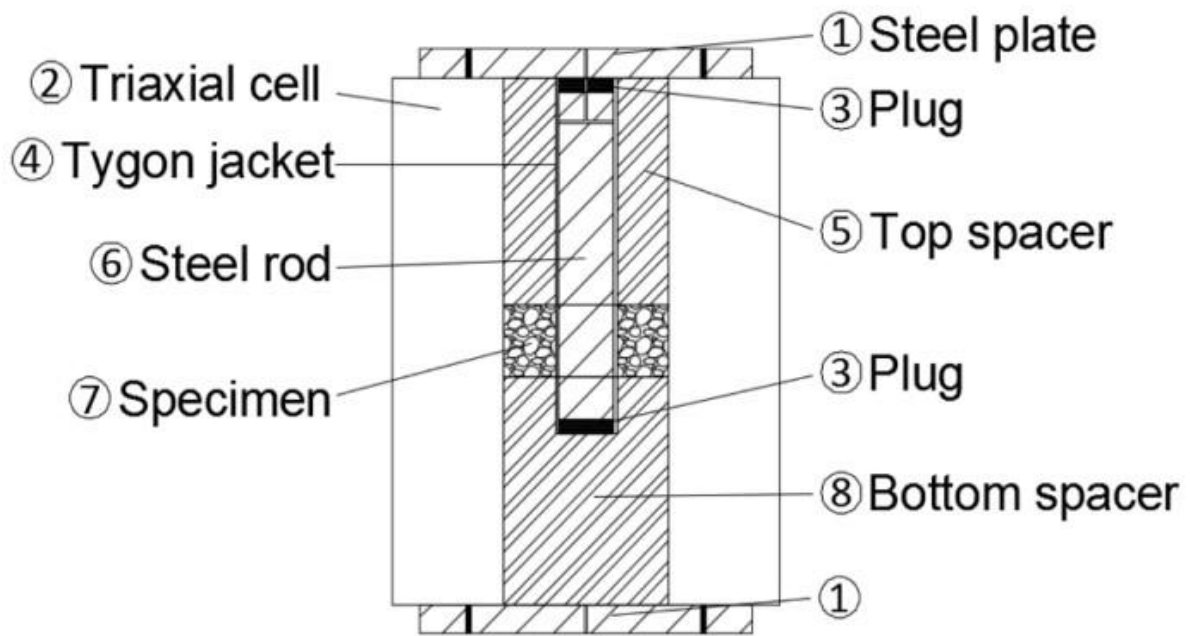
(a)
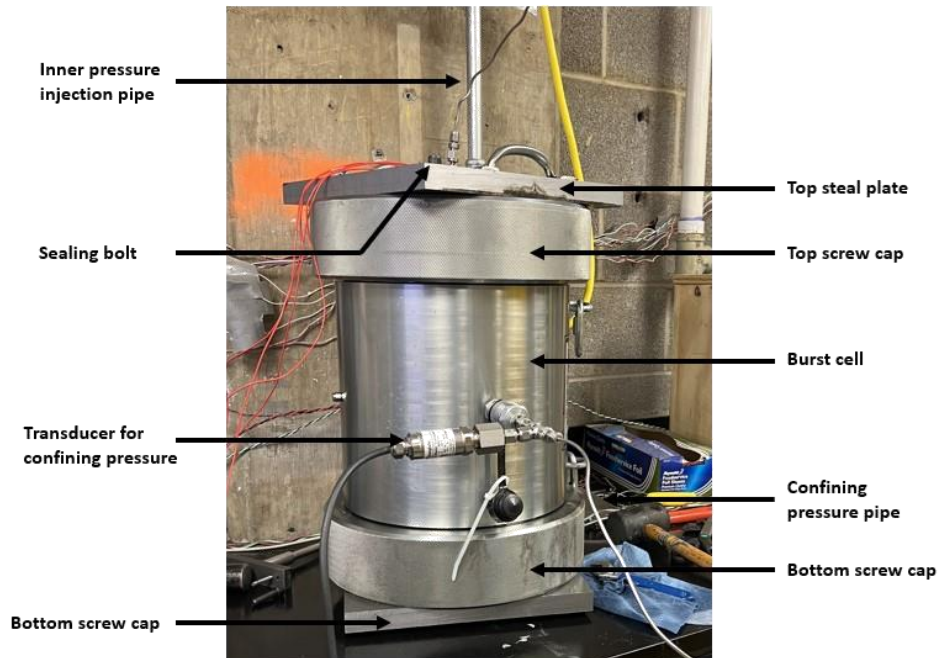
(b)

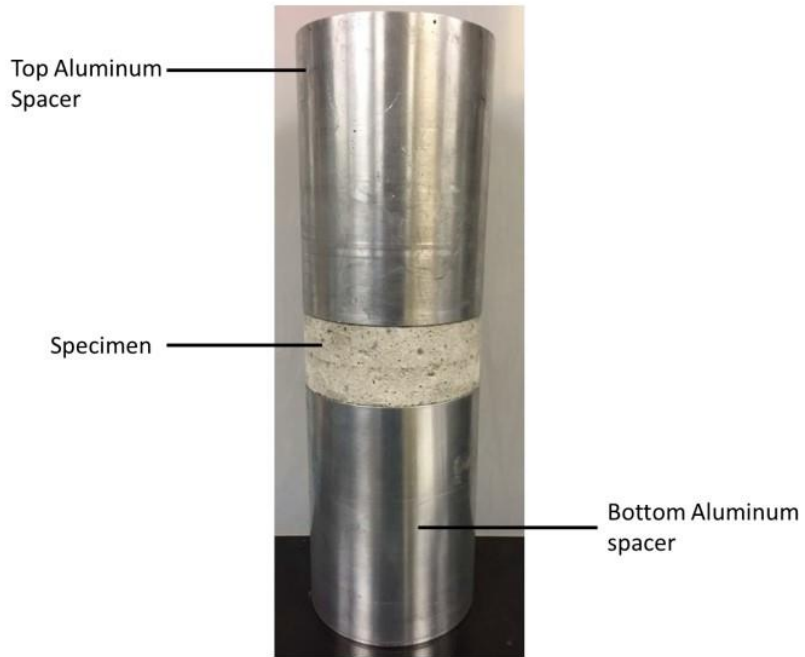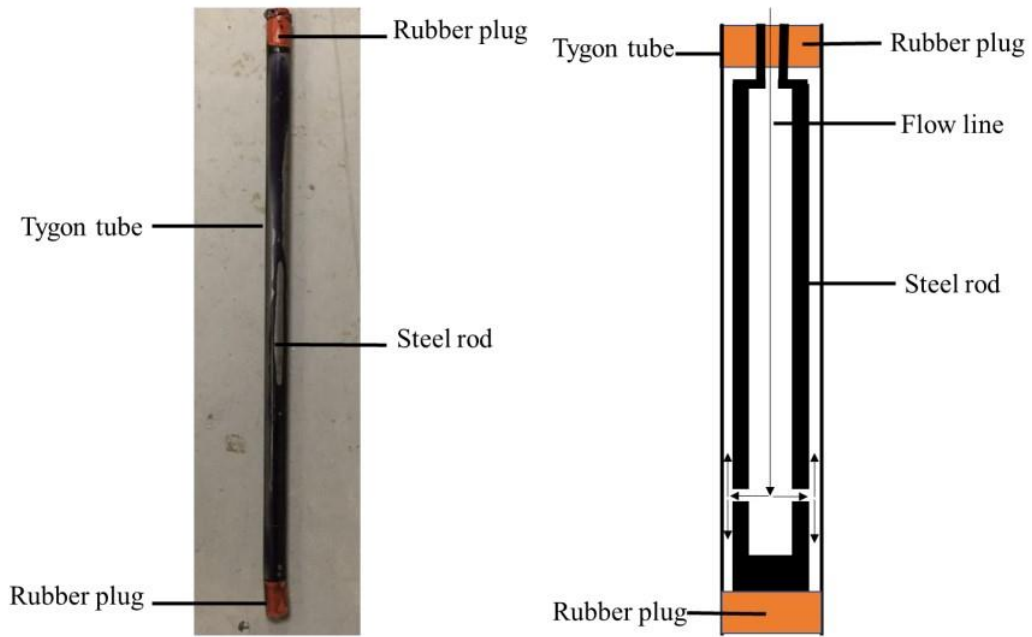Figure 3.1: a) Apparatus design for burst experiment (after Abou-Sayed, 1978) b) burst cell

Figure 3.2: (a) Spacers and sample for tests b) Tygon tube to apply inner pressure and rubber plug for system sealing (Zhang, 2019)

The proposed design of burst experiments is shown in Table 3.1 and Table 3.2. There are two different inner hole diameters: 12.7 mm (w = 12) and 50.8 mm (w = 3). The outer and inner pressure ratios are set to be 0, 1/6, and 1/8. The stability is assigned based on the global stability criterion (Section 2.2).

Table 3.1: Design of burst experiment configuration (the "Stability" column is based on global stability criterion (see Section 2.2))

Test Name	Stability	Hole Radius (mm)	W (b/a)	p* (P_o/P_i)	p*w
1, AE	unstable	6.35	12	0	0
2, AE	stable	6.35	12	1/8	1.5
3, AE	stable	6.35	12	1/6	2
4	unstable	25.4	3	0	0
5, AE	unstable	25.4	3	1/8	0.375
6	unstable	25.4	3	1/6	0.5
7	unstable	25.4	3	1/6	0.5

Table 3.2: Design of fixed confinement test configuration (the "Stability" column is based on global stability criterion (see Section 2.2))

| Test Name	Stability	Fixed (P_o)	W (b/a)	p* (P_o/P_i)	p*w
F-1	Stable /Unstable	1	12	0.05	0.60
F-2	Stable	3	12	0.08	0.96
F-3	Stable	4.8	12	0.09	1.08
F-4	Unstable	0.5	3	0.09	0.27
F-5	Unstable	3.5	3	0.27	0.81
F-6	Unstable	6.5	3	0.31	0.93

3.2 Sample Preparation

Kasota Valley Limestone is used in the course of these experiments and is a dolomitic limestone found and quarried in southern Minnesota, especially near the Minnesota River and its tributaries. Table 3.3 displays the measured rock properties of this limestone in the laboratory (G. Lu et al., 2020; Q. Lu et al., 2018).

Table 3.3: Material properties of Kasota Valley Limestone

Material property		Testing method
Young's modulus (GPa)	45	Uniaxial compression on cylindrical specimens (ASTME111-04, 2010a)
Poisson's ratio	0.3	Uniaxial compression on cylindrical specimens (ASTME132-04, 2010b)
Fracture toughness ($MPa\sqrt{m}$)	0.77	Three-point bending test on semicircular specimens (Kuruppu et al., 2014)

The sample preparation process begins by cutting 152.4x152.4x152.4 mm cube samples (Figure 3.3a) into half on a water saw (Figure 3.3b). Afterwards, it is cut into a cylindrical shape with an outer diameter of 152.4 mm in the core drill. These are then again core drilled to give either a 12.7 mm or 50.8 mm diameter central hole (Figure 3.3c). Following this, surface grinding (Figure 3.3d) is applied until 63.5 mm thick samples are achieved with a parallel and flat surface. Lastly, a wire saw (as illustrated in Figure 3.3e) is utilized to cut two diametrically opposed (bi-wing) notches, each with a length of 7.62 mm. The eventual shape of the prepared samples is given in Figure 3.4.
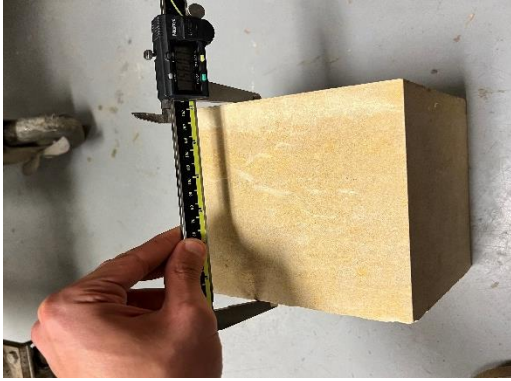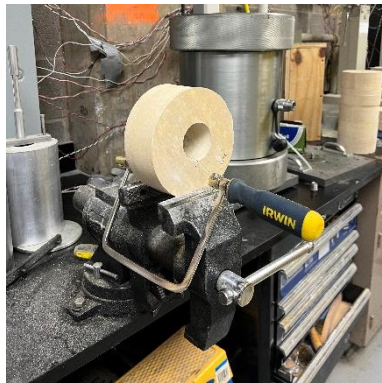
(a)

(b)

(c)

(d)

(e)

Figure 3.3: a) Cube sample, b) Water saw, c) Core drilling, d) Grinding machine, e) Wire saw
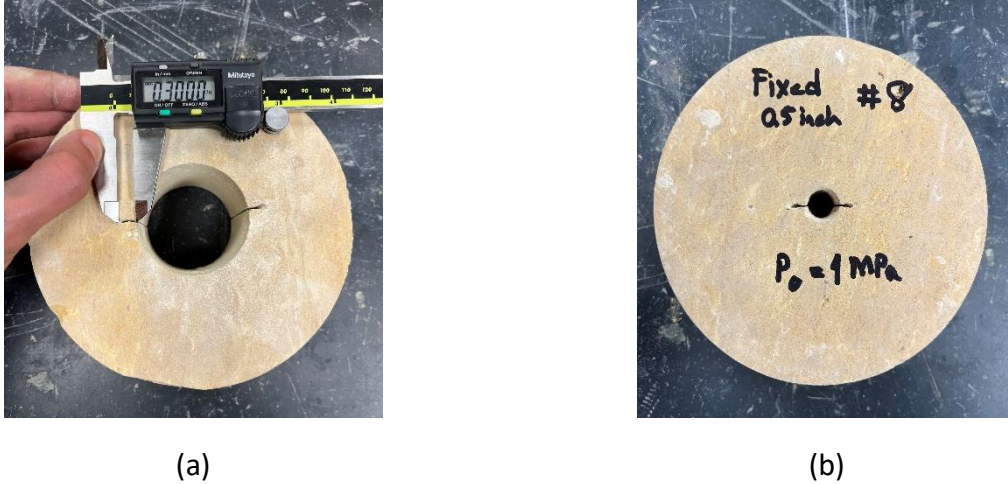
(a)   (b)

Figure 3.4: a) Limestone sample with 12.7mm inner hole b) Limestone sample with 50.8 mm central inner hole

3.3 Burst Experiment Procedure

The experimental setup necessitates substantial modifications when changing the aspect ratio parameter w. Therefore, we specifically focus on two values: $w = 12$ (with a 12.7 mm central hole) and $w = 3$ (with a 50.8 mm central hole). The experimental setups involve the utilization of configurations that are either stable or unstable in alignment with the global stability criterion described in Section 2.2. Stable configurations use a 12.7 mm central hole ($w = 12$) with pressure ratios $p* = 1/8$ and 1/6, whereas unstable configurations use a 12.7 mm central hole ($w = 12$) with $p* = 0$ and a 50.8 mm central hole ($w = 3$) with $p* = 0$, 1/8, and 1/6.

Initially, an aluminum spacer is placed at the base of the burst cell, followed by the placement of a tygon tube immediately (recall Figure 3.2b) with a steel rod inside below the center hole. After that, the limestone sample and a second aluminum spacer are put inside the burst cell through the tygon tube. The sealing of the system is achieved by placing a steel plate on the top of the cell, and the top rubber plug is precisely located within this plate to generate effective sealing. The connection of two ISCO syringe pumps is established, whereby one pump is connected to the burst cell to apply confining pressure, and the other pump is connected to the central tube to provide the inner pressure.

After completing all the necessary preparations, two ISCO syringe pumps are turned on simultaneously and set to pressure ramp rates to maintain a consistent ratio between the two pressures. The flow rate and the pressure are monitored until a sudden drop in pressure or increase in flow rate occurs.
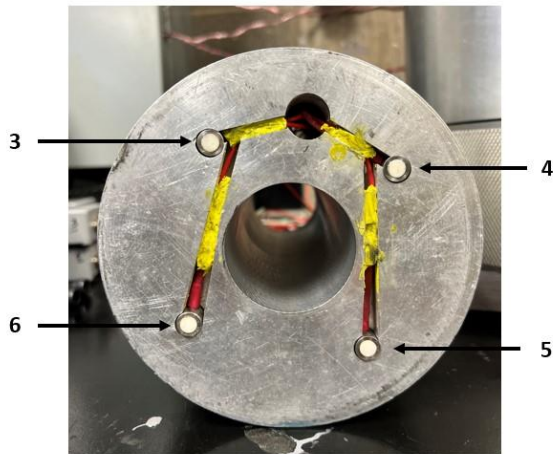
3.4 Accoustic Emission Monitoring

Yoshioka et al. (2023) proposed that the pressure peak signifies the ultimate failure of the sample rather than the initial crack propagation, when crack propagation is stable at the onset. This situation leads to severely overestimating fracture toughness. They have also pointed out that it might be possible to detect the onset of crack propagation through acoustic emission monitoring, although at the cost of reduced accuracy. Therefore, an acoustic emission (AE) monitoring system has also been applied in this study to show evidence of crack propagation well before rupturing the sample (Figure 3.5a).

Because of limitations in access within the burst cell, four sensors are strategically placed on the bottom surface of the top spacer (as shown in Figure 3.5b), ensuring direct contact with the top surface of the specimen. The positioning of the sensors can be seen in Figure 3.5b. Furthermore, as illustrated in Figure 3.5c, the direction of the notches induces the propagation of cracks between pairs of sensors. Thus, these four sensors function collectively to identify crack propagation, although they do not specify the precise location in the axial orientation of the sample. The collected data comprises the number of events changing over time, the location of each event, and the hit rate. Acoustic emission data is obtained as the internal pressure increases, showing the changing event counts over time. It is noteworthy to mention that the hit rate is calculated based on the number of times any channel is activated by a signal, while an event necessitates the activation of three channels simultaneously to receive hits. The analysis of AE monitoring results is done along with the pressure records to determine whether rock breakage occurred prior to the peak pressure.

(a)

(b)
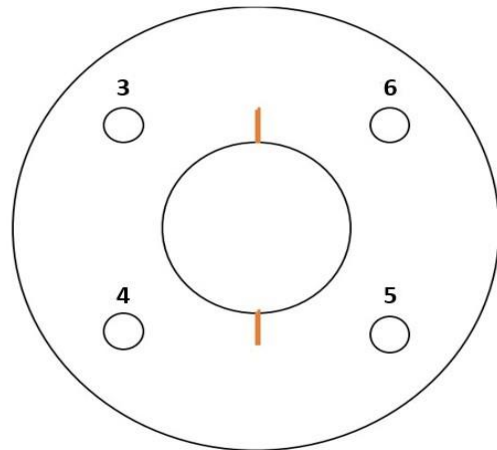
(c)

Figure 3.5: a) Acoustic emission monitoring system b) Sensors placed on the bottom of top spacer c) Sensor pattern (after Zhang, 2019)
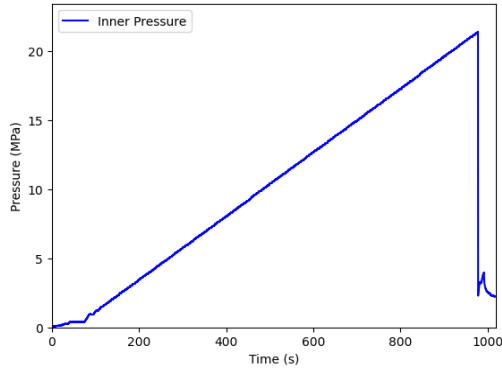
4 RESULTS OF EXPERIMENTS
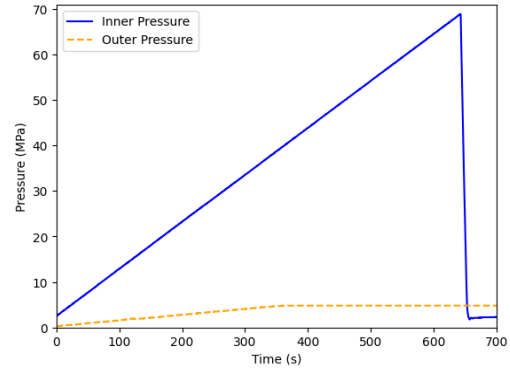
4.1 Burst Experiments with *w* =12

4.1.1 Pressure Results

In the first series of experiments, the geometry configuration is fixed with a 76.2 mm outer radius and a 6.35 mm inner hole radius, which means *w* = 12 (see Table 1). Thus, all parameters remain constant with the exception of *p**. Three different pressure ratios have been applied in these tests, namely *p** = 0, *p** = 1/8 and *p** = 1/6. Also, three tests are carried out with the AE monitoring. To begin with, the inner pressure is increased at a constant rate of 6.2 MPa/min, starting from 2.5 MPa, while simultaneously the outer (confining) pressure is increase at 1.03 MPa/min (1/6 of the rate of the inner pressure) from 0.42 MPa, or 0.78 MPa/min (1/8 of the rate of the inner pressure) from 0.31 MPa.

Figure 4.1a highlights the first unconfined test (*p** = 0, test 1), where the inner pressure reaches 21.42 MPa, after which the sample ruptures. This peak pressure is chosen as the critical point to estimate the fracture toughness via Equation (2.5). In other experiments with *p** = 1/6 and *p** = 1/8 (test 2) and (test 3) respectively, the inner pressure ramps up to 68.95 MPa (shown in Figure 4.1), then a sudden decrease occurs in inner pressure. This happens as the pumps reach their maximum capacity in these two experiments. Despite 68.95 MPa inner pressure, the samples do not burst. For this reason, peak pressure cannot be chosen to estimate K_{IC}. In a word, the critical inner pressure for each test has been chosen, corresponding to the pressure drop taken as evidence of the sample's rupture. The resulting estimate of K_{IC} will be presented in the next chapter.
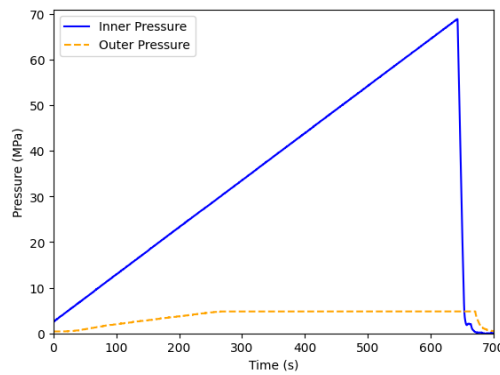
Figure 4.1: Pressure results for burst experiments with w = 12, (a) test 1 (unconfined), (b) test 2 (p*=1/8), (c) test 3 (p*=1/6)

4.1.1.1 AE Records

The SIF simulations predict that there will be stable growth for w = 12 with $p* > 0$. Hence, tests with $p*$ = 1/6 and 1/8 are presented here, which are predicted to have a period of stable growth before the rupture of the sample. Acoustic Emission (AE) monitoring results indicating significant generation of acoustic energy before the rupture of the sample will be taken as evidence of stable growth well before the peak pressure. Three sets of AE records for w = 12 are compared in this section: one from an unconfined test with unstable growth (Figure 4.2a), and two from confined tests with $p*$ = 1/8 and $p*$ = 1/6 that exhibited predicted stable growth (Figure 4.2b and c). The comparison of these series of records revealed a distinct difference, providing evidence of stable crack growth in the confined tests with $p*$ = 1/8 and $p*$ = 1/6. It is

clear that the number of events grows in a different way for these two different crack growth types. For the unconfined test, predicted to have only unstable growth, the number of events kept almost unchanged before the rupture of the sample. Then it suddenly increases, corresponding to the pressure drop point shown in Figure 4.2a. However, for the confined test with $p* = 1/8$, with predicted stable growth, the number of events steadily increases from 0 to above 200 over a period of about 600 seconds of loading (Figure 4.2b). Then it suddenly grows from 200 to upwards, corresponding to the rupture of the sample determined by the pressure drop point in Figure 4.2b. A test with $p* = 1/6$ has been run afterwards, also with predicted stable growth, and AE monitoring records during this test again show steady growth of the event number before the pressure peak. The number of events gradually increases from 0 to 18 over a period of 500 seconds of loading (Figure 4.2c). Then a sudden growth is shown from 18 upwards due to the sample's rupture at the pressure drop point, as illustrated in Figure 4.2c. The AE records demonstrate a clear distinction between stable and unstable growth, yet visual confirmation is necessary to validate the existence of stable fracture growth.
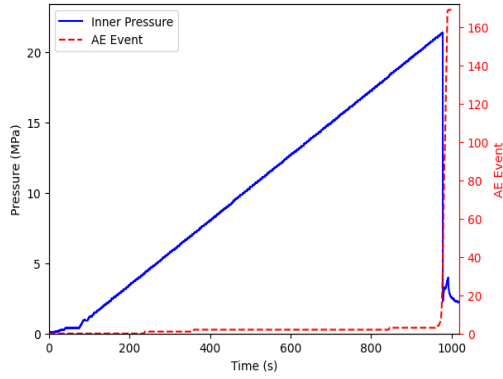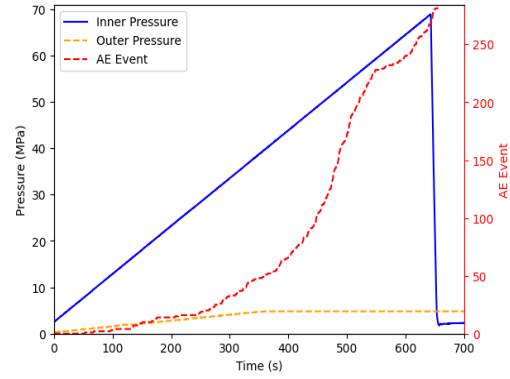
Figure 4.2 AE monitoring records corresponding to w = 12 tests, (a) test 1 (unconfined), (b) test 2 (p*=1/8), (c) test 3 (p*=1/6)

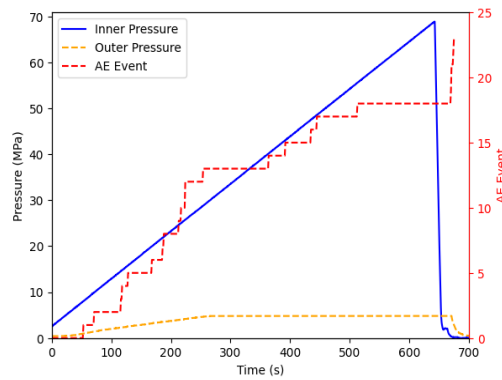## 4.2 Burst Experiments with w =3

4.2.1 Pressure Results

In contrast to the tests performed with w = 12, the burst tests involving w = 3 are anticipated to exhibit solely unstable crack propagation. These sets of burst experiments have been performed with varying pressure ratios, while keeping all other parameters constant, as outlined in Table 3.1. Thus, applying the same characteristics of all preceding tests, the initial internal pressure is 2.48 MPa, with a fixed rate of pressure increase at 6.2 MPa/min. The pressure ratio $p*$ (considered as 0, 1/8, and 1/6) stands out as the only variable in this series of

experiments, while the dimensions w and the initial crack length of each sample remain fixed. Figure 4.3 displays the pressure records obtained from all experiments for $w = 3$.

The unconfined test ($p^* = 0$, test 4) result with a sample having a 6.35 mm inner hole radius is shown in Figure 4.3a. The inner pressure increased up to 3.67 MPa, and then the sample ruptured from the initial notch. This peak pressure is selected to be the critical pressure to estimate fracture toughness. However, this test resulted in a higher peak pressure value than expected because the sample did not fail along the notch direction after half of the sample (Figure 4.4). Then, a typical confined test with $p^* = 1/8$ (test 5) is performed starting from 0.31 MPa, where the confining pressure was applied with an increase of 0.78 MPa/min (1/8 of the rate of the inner pressure). The inner pressure increases to 4.22 MPa (Figure 4.3b), after which the sample bursts. Finally, two confined tests with $p^* = 1/6$ (tests 6 and 7) are carried out with an initial confining pressure of 0.42 MPa, where the confining pressure is increased 1.03 MPa per minute (1/6 of the rate of the inner pressure). The peak pressure values of 5.79 MPa and 7.90 MPa are measured (Figure 4.3c and d), respectively, which are used to estimate K_{IC}. It is sometimes the case that the inner pressure ramps up even after the first sudden pressure drop, which leads to two or more peaks of inner pressure over a certain period. In this situation, it is questionable which peak pressure should be chosen to estimate the fracture toughness of the notch. Our approach is to choose the first peak pressure corresponding to initial growth to prevent any overestimation of the K_{IC} value.
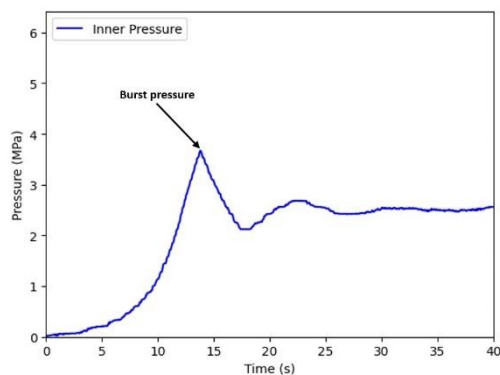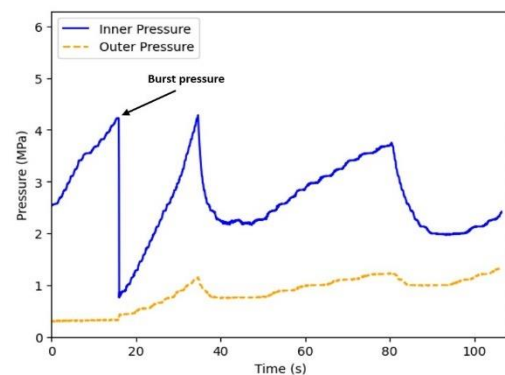
(a)   (b)

(c)
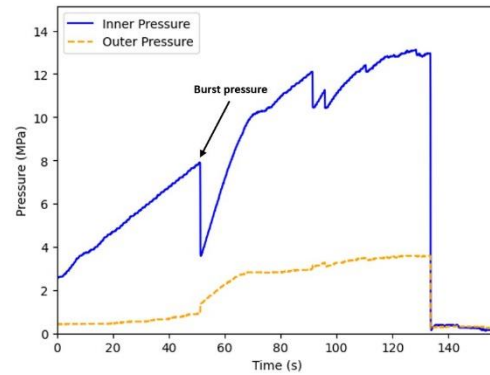
(d)

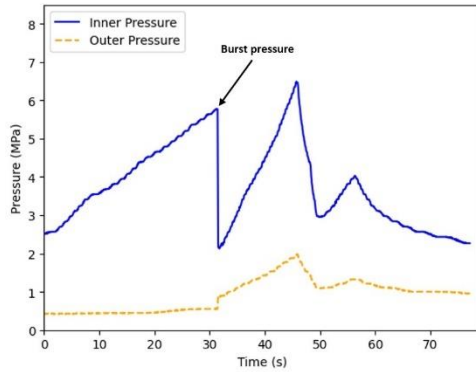Figure 4.3 : Pressure results for burst experiments with w = 3, (a) test 4 (unconfined), (b) test 5 (p*=1/8), (c) test 6 (p*=1/6), (c) test 7 (p*=1/6)
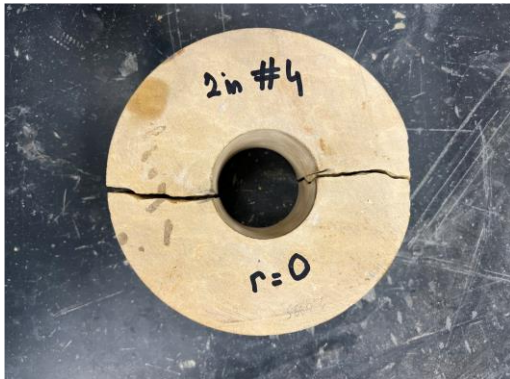
Figure 4.4: Unexpected crack growth after the half of the sample in unconfined test

4.2.1.1 AE Records

The AE records obtained from burst experiments with w = 12 reveal notable distinctions between unstable growth and stable growth (recall Figure 4.2). However, SIF computations predict only unstable growth for experiments with w = 3 configurations having $p*$ = 0, 1/8 and 1/6. Thus, it is valuable to analyze the behavior of unstable growth in these AE records to compare to those earlier experiments displaying potential stable growth.

For this reason, AE monitoring has been applied to the test with $p*$ = 1/8 for w = 3. The peak burst pressure has been chosen as 4.22 MPa. The AE records demonstrate similar results to the earlier test, showcasing unsteady growth only when w = 12 and $p*$ = 0. The AE records for this

31

single case show that the number of events is around 20 until a sudden drop in inner pressure is observed. Then the number of events dramatically increased to 300 (Figure 4.5). This spike in the number of events is a significant indicator of unstable growth at the time of rupture. This result here highlights the characteristics of the test with unstable growth from AE using a different geometry configuration. Nonetheless, the cause of the limited number of events that occurred at the early stage remains ambiguous, and it cannot be excluded that they could be associated with unforeseen stable crack growth.
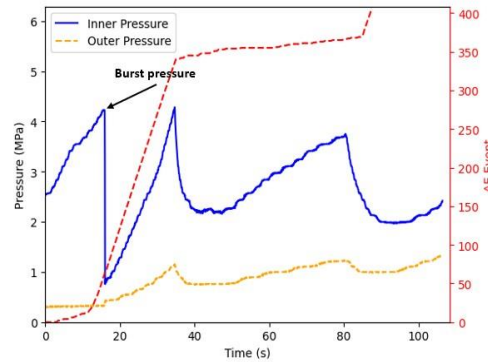

Figure 4.5: AE monitoring records corresponding to w = 3 tests having p^* = 1/8

4.3 Fixed Confinement Tests

The outer and inner pressures of the original burst experiment in Abou-Sayed (1978), increase proportionally, with a ratio of p^*. In previous tests, both the initial inner pressure and the initial notch length were fixed. Then those tests are designed to analyze the dependence on the pressure ratio p^* and the specimen configuration w. In this part, a series of tests with fixed confinement have been carried out to further evaluate the possible confining pressure dependence of the behavior from another perspective.

4.3.1 Results with w =12

Three levels of outer pressure have been applied for tests with the same geometry (w = 12), namely 1 MPa, 3 MPa, and 4.8 MPa. The pictures of samples after the rupture are illustrated together with the pressure monitoring results in Figure 4.6. The peak pressures, which have been chosen to be the critical points to estimate the K_{IC}, are 20.31 MPa, 37.19 MPa, and 53.87 MPa, respectively.
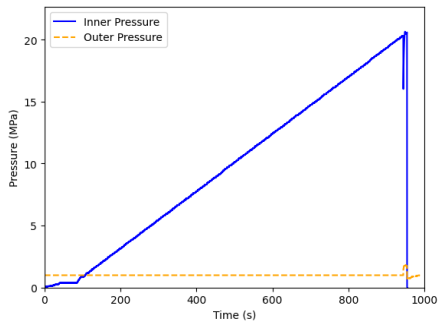
(a)
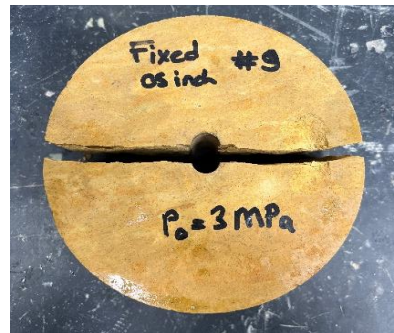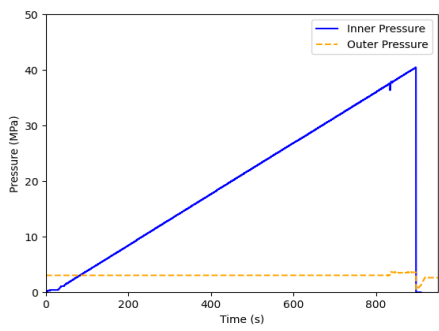
(b)
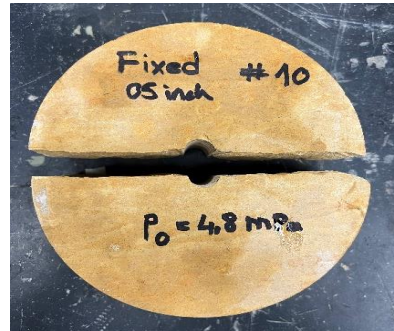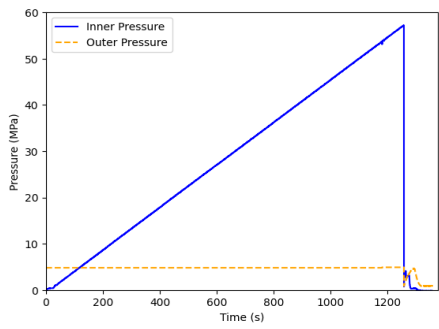
(c)

Figure 4.6: Tests with fixed confinement for *w* = 12 as, (a) 1 MPa (F-1), b) 3 MPa (F-2), c) 4.8 MPa (F-3)

4.3.2 Results with $w =3$

Three levels of outer pressure have been applied for tests with the same geometry (w = 3), namely 0.5 MPa, 3.5 MPa, and 6.5 MPa. For all these experiments, inner pressure has shown a steady increase until the point of rupture. The broken samples and the pressure monitoring results are shown in Figure 4.7. The peak pressure results are considerably lower compared to burst pressures achieved in the previous section with w = 12 geometry. The peak pressures, which have been chosen to be the critical points to estimate the K_{IC}, are 5.66 MPa, 13.05 MPa, and 21.25 MPa, respectively.

(a)

(b)
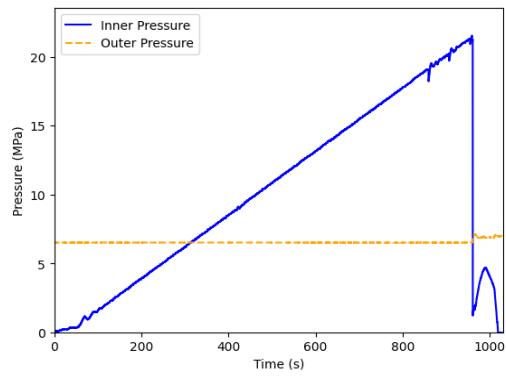
(c)

Figure 4.7: Tests with fixed confinement for w = 3 as, (a) 0.5 MPa (F-4), b) 3.5 MPa (F-5), c) 6.5 MPa (F-6)

5 FRACTURE TOUGHNESS (K_{IC}) ESTIMATION

5.1 K_{IC} Calculation

The facture toughness of the burst experiment is determined by the critical pressure at the point of burst, geometry, and computed SIF results, as described in Section 2. The fracture toughness is estimated for the experiments with w = 3 and w = 12 configurations, and a fixed confinement pressure. The critical i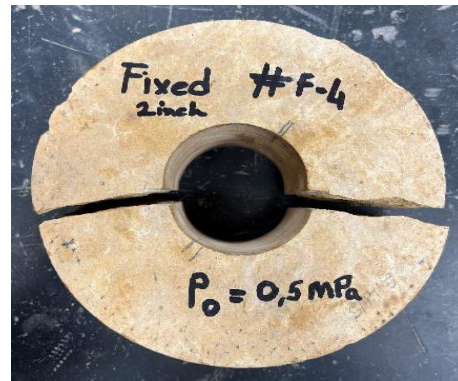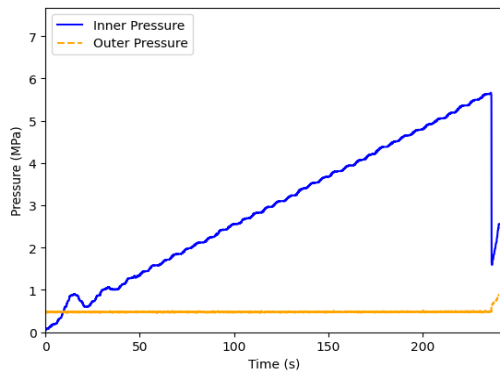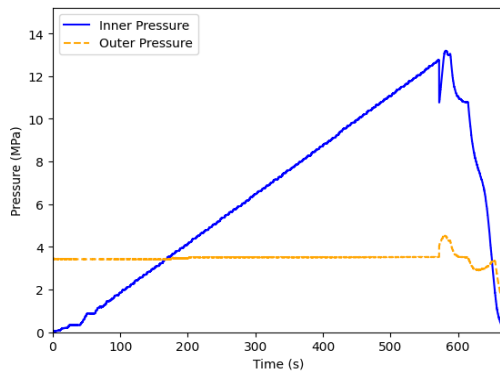nner pressure point has been identified for each test, as described in Section 4. In this chapter, K_{IC} is estimated for each case using Equation (2.5), with the results shown in Table 5.1. Moreover, for the tests with fixed confinement, K_{IC} results are shown in Table 5.2. It is obvious that K_{IC} varies significantly from 0.51 MPa$\sqrt{m}$ to 2.21 MPa$\sqrt{m}$. The fracture toughness estimations with proportional applied pressures in accordance with the original burst experiment setup are generally lower than those with a fixed confinement pressure. For the w = 3 tests with p^* = 1/6 and p^* = 1/8, (test 2) and (test 3) respectively, the K_{IC} value cannot be estimated, as the pump has reached its maximum value of 68.95 MPa and the experiment was stopped. The K_{IC} values have also shown a steady increase, as confining pressure is increased in fixed confinement pressure experiments.

Table 5.1: Summary of K_{IC} estimations for w = 3 and w = 12 experiments (note the "Stability" column is based on global stability criterion (see Section 2.2); "AE" means that test with AE monitoring)

Test Name	Stability	Hole Radius (mm)	w (b/a)	p^* (P_o/P_i)	p^*w	P_i (MPa)	K_{IC} (MPa$\sqrt{m}$)
1, AE	unstable	6.35	12	0	0	21.42	1.28
2, AE	stable	6.35	12	1/8	1.5	-	-
3, AE	stable	6.35	12	1/6	2	-	-
4	unstable	25.4	3	0	0	3.67	0.61
5, AE	unstable	25.4	3	1/8	0.375	4.22	0.51
6	unstable	25.4	3	1/6	0.5	5.79	0.62
7	unstable	25.4	3	1/6	0.5	7.90	0.85

Table 5.2: Summary of K_{IC} estimations for fixed confinement experiments (note the "Stability" column is based on global stability criterion (see Section 2.2); "AE" means that test with AE monitoring)

Test Name	Stability	Fixed (P_o)	w	r	p*w	P_i (MPa)	K_{IC} (MPa$\sqrt{m}$)
F-1	Stable /Unstable	1	12	0.05	0.60	20.31	1.00
F-2	Stable	3	12	0.08	0.96	37.19	1.59
F-3	Stable	4,8	12	0.09	1.08	53.87	2.21
F-4	Unstable	0,5	3	0.09	0.27	5.66	0.77
F-5	Unstable	3,5	3	0.27	0.81	13.05	0.97
F-6	Unstable	6,5	3	0.31	0.93	21.25	1.30

5.2 Dependence of Fracture Toughness on Confinement

5.2.1 Evaluation of $w = 3$ and $w = 12$ Tests

Previous burst experiments have provided evidence supporting the opinion that K_{IC} is influenced by the confining pressure (Figure 1.1). This section examines the possible dependence of K_{IC} on confinement in $w = 3$ and $w = 12$ burst experiments with possible stable and unstable growth. The comparison of the $w = 3$ and $w = 12$ test results is given in Figure 5.1. Unlike $w = 3$ burst experiments, all $w = 12$ tests are predicted to be unstable in global stability criterion. However, $w = 12$ tests with $p^* = 1/6$ and $p^* = 1/8$ are supposed to have stable crack growth. In the previous study of Yoshioka et al. (2023), it was shown that the K_{IC} of the test with $p^* = 1/8$ is larger than that of the test with $p^* = 1/6$, which is contrary to results from $w = 3$ tests. Since the pump capacity did not allow us to calculate K_{IC} with $w = 12$ tests having $p^* = 1/6$ and $p^* = 1/8$, they cannot be interpreted. However, K_{IC} of the $w = 3$ tests with $p^* = 1/6$ is greater than that of the test with $p^* = 1/8$, which confirms previous studies. Considering all these findings, it is challenging to interpret the relationship between fracture toughness and

confinement in stable experiments. The influence of confinement on K_{IC} becomes more evident in the burst experiments conducted with w = 3. The SIF simulation and the AE records indicate that w = 3 series of tests exhibits solely unstable crack growth. As it is already mentioned in Section 4.2.1. the K_{IC} of test 4 is higher than expected, as the sample failed in an unexpected way (recall Figure 4.4). Other than that, Figure 5.1 illustrates a clear linear positive correlation between K_{IC} and the confining stress, which is in agreement with the results reported in the literature.
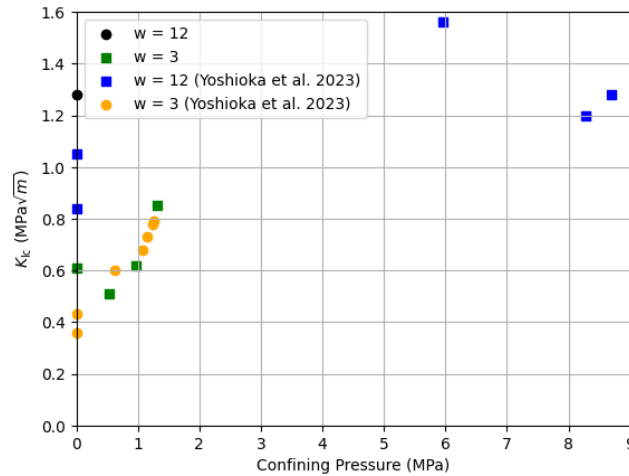

Figure 5.1: Fracture toughness K_{IC} as a function of the confining pressure P_o for w = 3 and w = 12

5.2.2 Evaluation of Fixed Confinement Tests

We will be focusing on investigating the dependence of K_{IC} on confinement and analyzing the results from fixed confinement tests. It should be noted that three distinct values of confining pressure are applied in the tests for two different configurations (w = 3 and w = 12). Since 1 MPa, 3 MPa, and 4.8 MPa confining pressures have already been applied on w = 3 geometry in Zhang (2019), the confining pressures have been adjusted to 0.5 MPa, 3.5 MPa, and 6.5 MPa on the same geometry in this study to expand the range of applications. But then, the same three values of confining pressure in Zhang (2019) are applied on the w = 12 configuration. When we compare the K_{IC} results with Zhang's study, it is seen that relatively higher K_{IC} values have been estimated in this study. This may be due to the differences in the characteristics of the samples taken. An anticipated phenomenon shows that when confining pressure is large enough, the K_{IC}

increases in contrast to the study of Zhang. It can be clearly seen that there is a linear correlation between increasing confining pressure and K_{IC} values. Considering the SIF computation results, tests with w = 3 configuration are proposed to show unstable crack growth, whereas tests with w = 12 are mostly expected to have stable crack growth. According to the results of this study, there appears to be a linear positive correlation between K_{IC} values and confining pressure, if the same crack growth type is expected for either w = 3 or w = 12 configurations. One important point is to consider might be that the SIF simulation result proposed unstable crack growth with 6.5 MPa confining pressure on w = 3 configuration, whereas Zhang (2019) shows stable crack growth with 4.8 MPa for the same configuration. This change in crack growth type with increasing confining pressure is difficult to interpret.
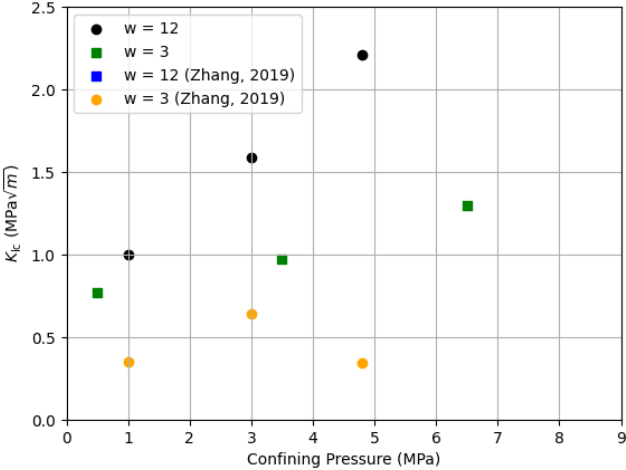

Figure 5.2: Fracture toughness K_{IC} as a function of the confining pressure with fixed confining pressure P_o for w =3 and w =12

6 CONCLUSION

This study focuses on the identification of stable crack growth in the burst experiment, illustrating its implications, and suggesting modifications to address the challenges it presents. The key contributions of this research can be summarized as follows:

The characteristics of AE monitoring records provide valuable insights in terms of investigating crack growth. Generally, the records obtained from tests predicting stable growth exhibit dissimilar characteristics compared to those predicting only unstable growth. Over time, the stable growth tests demonstrate a gradual and continuous increase in the number of events, whereas the number of events increases remarkably at the point of burst with unstable growth tests. The acoustic emission monitoring method demonstrated that stable crack propagation normally occurs well before the final failure, which leads to an overestimation of fracture toughness when it is calculated using the peak pressure result according to the original test procedure. In order to ensure accurate estimation of K_{IC} and to avoid the possibility of spurious dependence of fracture toughness on confining stress, it is preferable to use unstable configurations. It is crucial to conduct additional research on the existence of stable crack growth. One possible investigation might be artificially stopping a burst experiment just before the point of rupture and then cutting the sample layer by layer. This method could offer more insights compared to the current procedure. This meticulous analysis may reveal visible evidence that definitively proves the presence of stable growth. Another possibility might be the use of developed sensor distribution or a method, which enables researchers to detect reliable location of the events over the experiments.

The relationship between K_{IC} and confinement has been examined through proportional pressurized and fixed confinement experiments. When considering only unstable growth a linear positive correlation is observed between K_{IC} and confining pressure. Addition to this, positive relationship between K_{IC} and confinement is also observed considering the results of fixed confinement tests.

The global criterion of stability predictions has been compared and verified with the recordings of AE monitoring system. The SIF predictions generally showed the correct type of stable and unstable crack growth.

In summary, the AE records indicate a stable growth pattern prior to specimen rupture, potentially leading to inaccurate K_{IC} estimation. However, in cases of unstable crack growth, there is a direct positive correlation between K_{IC} and confining pressure for both proportional pressurized and fixed confinement tests. The criterion provided can be utilized in future research endeavors to develop burst experiments, followed by employing sophisticated analyses of AE outcomes. The implementation of further tests would contribute to a clearer comprehension of the nature of stable crack growth, as well as insights into the underlying mechanical factors and predictive capabilities concerning the fracture toughness estimations under confining pressure.

ACKNOWLEDGEMENTS

REFERENCES

Abou-Sayed. (1978). *An experimental technique for measuring the fracture toughness of rocks under downhole stress conditions*.

Bowie, O. L., & Freese, C. E. (1972). Elastic analysis for a radial crack in a circular ring. *Engineering Fracture Mechanics*, *4*(2), 315–321. https://doi.org/10.1016/0013-7944(72)90045-8

Clifton, R. J., Simonson, E. R., Jones, A. H., & Green, S. J. (1976). *Determination of the critical-stress-intensity factor from internally pressurized thick-walled vessels*.

Destuynder, P., Djaoua, P. E. M., Chesnay, L., & Nedelec, J. C. (1981). Sur une Interprétation Mathématique de l'Intégrale de Rice en Théorie de la Rupture Fragile. *Mathematical Methods in the Applied Sciences*, *3*(1), 70–87. https://doi.org/10.1002/mma.1670030106

Dubois, F., Chazal, C., & Petit, C. (1999). A Finite Element Analysis of Creep-Crack Growth in Viscoelastic Media. In *Mechanics of Time-Dependent Materials* (Vol. 2).

Gmsh: a three-dimensional finite element mesh generator with built-in pre- and post-processing facilities. (n.d.). Retrieved March 24, 2024, from https://gmsh.info/

Griffith, A. A. (1921). VI. The phenomena of rupture and flow in solids. *Philosophical Transactions of the Royal Society of London. Series A, Containing Papers of a Mathematical or Physical Character*, *221*(582–593), 163–198. https://doi.org/10.1098/rsta.1921.0006

Griffith, A. A. (1924). Griffith's Theory of Rupture. In C. B. Biezeno & J. M. Burgers (Eds.), *International Congress for Applied Mechanics* (pp. 55–63). J. Waltman.

Huang, Y., Zolfaghari, N., & Bunger, A. P. (2022). Cohesive element simulations capture size and confining stress dependence of rock fracture toughness obtained from burst experiments. *Journal of the Mechanics and Physics of Solids*, *160*. https://doi.org/10.1016/j.jmps.2022.104799

Irwin, G. R. (1957). Analysis of Stresses and Strains Near the End of a Crack Traversing a Plate. *Journal of Applied Mechanics*, *24*(3), 361–364. https://doi.org/10.1115/1.4011547

Kuruppu, M. D., Obara, Y., Ayatollahi, M. R., Chong, K. P., & Funatsu, T. (2014). ISRM-Suggested Method for Determining the Mode I Static Fracture Toughness Using Semi-Circular Bend Specimen. *Rock Mechanics and Rock Engineering*, *47*(1), 267–274. https://doi.org/10.1007/s00603-013-0422-7

Lu, G., Gordeliy, E., Prioul, R., Aidagulov, G., Uwaifo, E. C., Ou, Q., & Bunger, A. P. (2020). Time-Dependent Hydraulic Fracture Initiation. *Journal of Geophysical Research: Solid Earth*, *125*(3). https://doi.org/10.1029/2019JB018797

Lu, Q., Lu, G., Prioul, R., Aidagulov, G., & Bunger, A. P. (2018). Impact of Fluid Acidity on the Time-Dependent Initiation of Hydraulic Fractures in Carbonate Rocks. *Rock Mechanics and Rock Engineering*, *51*(12), 3895–3906. https://doi.org/10.1007/s00603-018-1544-8

M. Erwan Tanné. (2017). *Variational phase-field models from brit- tle to ductile fracture: nucleation and propagation.* [PhD Thesis]. Université Paris-Saclay, École Polytechnique.

OpenGeoSys. (n.d.). Retrieved March 24, 2024, from https://www.opengeosys.org/

Stress intensity factor - Wikipedia. (n.d.). Retrieved March 24, 2024, from https://en.wikipedia.org/wiki/Stress_intensity_factor

Suo, X.-Z., & Combescure, A. (1992). On the application of G(Θ) method and its comparison with De Lorenzi's approach. *Nuclear Engineering and Design*, *135*(2), 207–224. https://doi.org/10.1016/0029-5493(92)90223-I

Yoshioka, K., Zhang, Y., Lu, G., Bunger, A., Adachi, J., & Bourdin, B. (2023). Improving the Accuracy of Fracture Toughness Measurement in Burst Experiments. *Rock Mechanics and Rock Engineering*, *56*(1), 427–436. https://doi.org/10.1007/s00603-022-03097-y

Zhang, Y. (2019). *Title Page Stress Dependence of the Burst Experiment for Determining Fracture Toughness*.